

Big bang nucleosynthesis constraints on scalar-tensor theories of gravity

Alain Coc*

*Centre de Spectrométrie Nucléaire et de Spectrométrie de Masse,
IN2P3/CNRS/UPS, Bât. 104, 91405 Orsay Campus (France)*

Keith A. Olive†

William I. Fine Theoretical Physics Institute, University of Minnesota, Minneapolis, MN 55455 (USA)

Jean-Philippe Uzan‡ and Elisabeth Vangioni§

*Institut d'Astrophysique de Paris, UMR-7095 du CNRS,
Université Pierre et Marie Curie, 98 bis bd Arago, 75014 Paris (France)*

(Dated: March 20, 2022)

We investigate BBN in scalar-tensor theories of gravity with arbitrary matter couplings and self-interaction potentials. We first consider the case of a massless dilaton with a quadratic coupling to matter. We perform a full numerical integration of the evolution of the scalar field and compute the resulting light element abundances. We demonstrate in detail the importance of particle mass thresholds on the evolution of the scalar field in a radiation dominated universe. We also consider the simplest extension of this model including a cosmological constant in either the Jordan or Einstein frame.

PACS numbers: PACS

I. INTRODUCTION

The concordance model of cosmology calls for the introduction of a cosmological constant or a dark energy sector. Various candidates have been proposed [1], among which the possibility that gravity is not described by general relativity on large cosmological scales. It is of interest therefore, to test our theory of gravity in a cosmological context. This can be achieved in two complementary ways, either by designing model independent tests (see e.g. Refs. [2, 3, 4] for a discussion of the various possible tests) or by considering a class of well motivated theories and use all available data to determine how close to general relativity we must be.

Among all extensions of general relativity, scalar-tensor theories are probably the simplest in the sense that they consider only the introduction of one [5] (or many [6]) scalar field(s) universally coupled to matter. These theories involve two free functions describing the coupling of the scalar field to matter and its self-interaction potential. They respect local Lorentz invariance and the universality of free fall of laboratory-size bodies. They are motivated by high-energy theories trying to unify gravity with other interactions which generically involve a scalar field in the gravitational sector. In particular, in superstring theories [7] the supermultiplet of the 10-dimensional graviton contains a scalar field,

the dilaton, and other scalar fields, moduli, appear during Kaluza-Klein dimensional reduction of higher dimensional theories to our usual four dimensional spacetime.

In cosmology, two main properties make these theories appealing. First, an attraction mechanism toward general relativity [8, 9] was exhibited. This implies that even if the tests of general relativity in the Solar system set strong constraints on these theories, they may differ significantly from general relativity at high redshift. Second, it was shown that the general mechanism of quintessence was conserved [10, 11] if the quintessence field was non-minimally coupled and that the attraction mechanism toward general relativity still held with runaway potentials [12, 13, 14]. These extended quintessence models are the simplest theories in which there is a long range modification of gravity, since the quintessence field is light, and they allow for a very interesting phenomenology [15].

Cosmological data give access to various aspects of these models. The cosmic microwave background (CMB) tests the theory in the linear regime [16, 17, 18, 19, 20] while weak lensing opens a complementary window on the non-linear regime [21, 22]. Solar system experiments give information on the theory today and big-bang nucleosynthesis (BBN) allows us to constrain the attraction mechanism toward general relativity [8] at very high redshift.

BBN is one of the most sensitive available probes of the very early Universe and of physics beyond the standard model. Its success rests on the concordance between the observational determinations of the light element abundances of D, ^3He , ^4He , and ^7Li , and their theoretically predicted abundances [23, 24]. Furthermore,

*Electronic address: coc@csnsm.in2p3.fr

†Electronic address: olive@physics.unm.edu

‡Electronic address: uzan@iap.fr

§Electronic address: vangioni@iap.fr

measurements of the CMB anisotropies by WMAP [25] have led to precision determinations of the baryon density or equivalently the baryon-to-photon ratio, η . As η is the sole parameter of the standard model of BBN, it is possible to make very accurate predictions [26, 27, 28, 29, 30] and hence further constrain physics beyond the standard model [31].

In particular, the ^4He abundance is often used as a sensitive probe of new physics. This is due to the fact that nearly all available neutrons at the time of BBN end up in ^4He and the neutron-to-proton ratio is very sensitive to the competition between the weak interaction rate and the expansion rate. Of interest to us here is the effect of modifications to gravity which will directly affect the expansion rate of the Universe through a modified Friedmann equation.

The WMAP best fit assuming a varying spectral index is $\Omega_b h^2 = 0.0224 \pm 0.0009$ and is equivalent to $\eta_{10, \text{CMB}} = 6.14 \pm 0.25$, where $\eta_{10} = 10^{10} \eta$. Using the WMAP data to fix the baryon density, the light element abundances [26, 27, 28, 29, 30] can be quite accurately predicted. Some BBN results are displayed in Table 1.

The effect of scalar-tensor theories of gravity on the production of light elements has been investigated extensively (see e.g. Ref. [32] for a review). As a first step, it is useful to consider only the speed up factor, $\xi = H/H_{\text{GR}}$, that arises from the modification of the value of the gravitational constant during BBN [31, 33]. Other approaches considered the full dynamics of the problem but restricted themselves to the particular class of Jordan-Fierz-Brans-Dicke theory [34], of a massless dilaton with a quadratic coupling [35, 36] or to a general massless dilaton [37]. It should be noted that a combined analysis of BBN and CMB data was investigated in Ref. [38] and Ref. [39]. The former considered G constant during BBN while the latter focused on a non-minimally quadratic coupling and a runaway potential. We stress that the dynamics of the field can modify CMB results so that one needs to be careful while inferring Ω_b from WMAP.

The goal of this article is to implement scalar-tensor theories in an up-to-date BBN code. This will complement our existing set of tools which allows us to confront scalar-tensor theories with observations of type Ia supernovae and CMB anisotropies [16] as well as weak lensing [21]. In particular, the predictions to be compared with observations can be computed in the same framework for any self-interaction potential and matter-coupling function.

We first recall, in § II, the equations describing the theory to be implemented in our BBN code and we also discuss local constraints. As a check of our code, we consider, in § III, the case of a massless dilaton with quadratic coupling [35]. In particular, we perform a full numerical integration up to the present that can be compared with the analytical results of Ref. [35]. We update the constraints on this model by taking into account the latest BBN data discussed above. We reaffirm that only

helium-4 is sensitive to the modification of gravity considered here. In § IV, we will consider the simplest extension of this model by introducing a cosmological constant. Such a constant can be introduced as a constant potential either in the Einstein frame, hence keeping the dilaton massless, or in the Jordan frame, hence generalizing the constant energy density component. Both cases are considered and we conclude in Section V. Applications to various cases of cosmological interest will be presented in a follow-up article.

II. IMPLEMENTING SCALAR-TENSOR THEORIES OF GRAVITY IN A BBN CODE

A. Scalar-tensor theories in brief

In scalar-tensor theories of gravity, gravity is mediated not only by a spin-2 graviton but also by a spin-0 scalar field that couples universally to matter fields. In the Jordan frame, the action of the theory takes the form

$$S = \int \frac{d^4x}{16\pi G_*} \sqrt{-g} [F(\varphi)R - g^{\mu\nu}Z(\varphi)\varphi_{,\mu}\varphi_{,\nu} - 2U(\varphi)] + S_m[g_{\mu\nu}; \psi] \quad (1)$$

where G_* is the bare gravitational constant from which we define $\kappa_* = 8\pi G_*$. This action involves three arbitrary functions (F , Z and U) but only two are physical since there is still the possibility to redefine the scalar field. F needs to be positive to ensure that the graviton carries positive energy. S_m is the action of the matter fields that are coupled minimally to the metric $g_{\mu\nu}$ with signature $(-, +, +, +)$.

The action (1) can be rewritten in the Einstein frame by performing the conformal transformation

$$g_{\mu\nu}^* = F(\varphi)g_{\mu\nu} \quad (2)$$

as

$$S = \int \frac{d^4x}{16\pi G_*} \sqrt{-g_*} [R_* - 2g_*^{\mu\nu}\partial_\mu\varphi_*\partial_\nu\varphi_* - 4V(\varphi_*)] + S_m[A^2(\varphi_*)g_{\mu\nu}^*; \psi]. \quad (3)$$

The field φ_* and the two functions $A(\varphi_*)$ and $V(\varphi_*)$ are defined by

$$\left(\frac{d\varphi_*}{d\varphi}\right)^2 = \frac{3}{4} \left[\frac{d \ln F(\varphi)}{d\varphi}\right]^2 + \frac{Z(\varphi)}{2F(\varphi)} \quad (4)$$

$$A(\varphi_*) = F^{-1/2}(\varphi) \quad (5)$$

$$2V(\varphi_*) = U(\varphi)F^{-2}(\varphi). \quad (6)$$

We will denote any Einstein frame quantities by a star (*), e.g. R_* is the Ricci scalar of the metric $g_{\mu\nu}^*$. The strength of the coupling of the scalar field to the matter fields is characterized by

$$\alpha(\varphi_*) \equiv \frac{d \ln A}{d\varphi_*} \quad (7)$$

TABLE I: BBN results for the light element abundances assuming the WMAP-inferred baryon density.

Source	Y_p	D/H $\times 10^{-5}$	$^3\text{He}/\text{H}$ $\times 10^{-5}$	$^7\text{Li}/\text{H}$ $\times 10^{-10}$
Coc <i>et al.</i> (2004)	0.2479 ± 0.0004	2.60 ± 0.17	1.04 ± 0.04	4.15 ± 0.46
Cybert <i>et al.</i> (2003)	$0.2484^{+0.0004}_{-0.0005}$	$2.74^{+0.26}_{-0.16}$	$0.93^{+0.1}_{-0.67}$	$3.76^{+1.03}_{-0.38}$

and we also define

$$\beta(\varphi_*) \equiv \frac{d\alpha}{d\varphi_*}. \quad (8)$$

It is useful to study both the Einstein and Jordan frames. In the Jordan frame, matter is universally coupled to the metric. The Jordan metric defines the length and time as measured by laboratory apparatus so that all observations (time, redshift,...) have their standard interpretation in this frame. However, to discuss the theory it is often better to use the Einstein frame in which the kinetic terms have been diagonalized so that the spin-2 and spin-0 degrees of freedom of the theory are perturbations of $g_{\mu\nu}^*$ and φ_* respectively. The physical properties of both frames are of course identical. For example, when we refer to the time variation of the gravitational constant (in the Jordan frame), we have assumed fixed particle masses. In contrast, in the Einstein frame, we would infer a fixed gravitational constant and varying masses. In both frames, the quantity Gm^2 (which is physically measureable) varies in the same way.

B. Friedmann equations

1. Equations in Jordan frame

We consider a Friedmann-Lemaître universe with metric in the Jordan frame

$$ds^2 = -dt^2 + R^2(t)\gamma_{ij}dx^i dx^j \quad (9)$$

where γ_{ij} is the spatial metric and R the scale factor. The matter fields are described by a collection of perfect fluids of energy density, ρ and pressure P . It follows that the Friedmann equations in Jordan frame take the form

$$\begin{aligned} 3F \left(H^2 + \frac{K}{R^2} \right) &= 8\pi G_* \rho + \frac{1}{2} Z \dot{\varphi}^2 - 3H\dot{F} + U(10) \\ -2F \left(\dot{H} - \frac{K}{R^2} \right) &= 8\pi G_*(\rho + P) + Z\dot{\varphi}^2 \\ &\quad + \ddot{F} - H\dot{F} \end{aligned} \quad (11)$$

where a dot refers to a derivative with respect to the cosmic time t and $H \equiv d \ln R / dt$. The Klein-Gordon

and conservation equations are given by

$$Z(\ddot{\varphi} + 3H\dot{\varphi}) = 3F_\varphi \left(\dot{H} + 2H^2 + \frac{K}{R^2} \right) - \frac{1}{2} Z_\varphi \dot{\varphi}^2 - U_\varphi \quad (12)$$

$$\dot{\rho} + 3H(\rho + P) = 0. \quad (13)$$

If we define the density parameters today by

$$\Omega_0 \equiv \frac{8\pi G_* \rho_0}{3H_0^2 F_0}, \quad (14)$$

the evolution of the energy density of a fluid with constant equation of state $w = P/\rho$ takes the usual form

$$\rho = \frac{3H_0^2 F_0 \Omega_0}{8\pi G_*} (1+z)^{3(1+w)} \quad (15)$$

where z is the redshift defined by $1+z = R_0/R$.

2. Equations in Einstein frame

The scale factor and cosmic time in Einstein frame are related to the ones in Jordan frame by

$$R = A(\varphi_*) R_*, \quad dt = A(\varphi_*) dt_* \quad (16)$$

so that the redshifts are related by

$$1+z = \frac{A_0}{A} (1+z_*). \quad (17)$$

The Friedmann equations in this frame take the form

$$\begin{aligned} 3 \left(H_*^2 + \frac{K}{R_*^2} \right) &= 8\pi G_* \rho_* + \psi_*^2 + 2V(\varphi_*) \quad (18) \\ -\frac{3}{R_*^2} \frac{d^2 R_*}{dt_*^2} &= 4\pi G_*(\rho_* + 3P_*) + 2\psi_*^2 - 2V(\varphi_*) \quad (19) \end{aligned}$$

where we have introduced $H_* = d \ln R_*/dt_*$ and

$$\psi_* = d\varphi_*/dt_*. \quad (20)$$

These equations take the same form as the standard Friedmann equations for a universe containing a perfect fluid and a scalar field. The Klein-Gordon equation takes the form

$$\frac{d\psi_*}{dt_*} + 3H_* \psi_* = -\frac{dV}{d\varphi_*} - 4\pi G_* \alpha(\varphi_*) (\rho_* - 3P_*) \quad (21)$$

while the matter conservation equation is given by

$$\frac{d\rho_*}{dt_*} + 3H_*(\rho_* + P_*) = \alpha(\varphi_*)(\rho_* - 3P_*)\psi_*. \quad (22)$$

These equations differ from their standard form due to the coupling that appears in the r.h.s. The solution of the evolution equation (22) can be obtained from the relation between the energy density and the pressure of a fluid in Einstein frame and their Jordan frame counterparts

$$\rho_* = A^4 \rho, \quad P_* = A^4 P \quad (23)$$

which imply, in particular, that

$$\rho_* = \frac{3H_0^2 \Omega_0}{8\pi G_*} \left(\frac{A}{A_0} \right)^{4-3(1+w)} (1+z_*)^{3(1+w)} \quad (24)$$

for a fluid with a constant equation of state.

C. Constraints today

1. Post-newtonian constraints

The post-Newtonian parameters (see Refs. [40, 45]) can be expressed in terms of the values of α and β today as

$$\gamma^{\text{PPN}} - 1 = -\frac{2\alpha_0^2}{1 + \alpha_0^2}, \quad \beta^{\text{PPN}} - 1 = \frac{1}{2} \frac{\beta_0 \alpha_0^2}{(1 + \alpha_0^2)^2}. \quad (25)$$

Solar System experiments set strong limits on these parameters. The perihelion shift of Mercury implies [41]

$$|2\gamma^{\text{PPN}} - \beta^{\text{PPN}} - 1| < 3 \times 10^{-3}, \quad (26)$$

the Lunar Laser Ranging experiment [42] sets

$$4\gamma^{\text{PPN}} - \beta^{\text{PPN}} - 3 = -(0.7 \pm 1) \times 10^{-3}. \quad (27)$$

Two experiments give a bound on γ^{PPN} alone, the Very Long Baseline Interferometer [43]

$$|\gamma^{\text{PPN}} - 1| < 4 \times 10^{-4}, \quad (28)$$

and the measurement of the time delay variation to the Cassini spacecraft near Solar conjunction [44]

$$\gamma^{\text{PPN}} - 1 = (2.1 \pm 2.3) \times 10^{-5}. \quad (29)$$

These two last bounds imply α_0 to be very small, typically $\alpha_0^2 < 10^{-5}$ while β_0 can still be large [46]. Binary pulsar observations impose that $\beta_0 \gtrsim -4.5$. Note that even though β_0 is not bounded above by experiment, we will assume that it is not very large, typically we assume $\beta_0 \lesssim 100$, so that the post-Newtonian approximation scheme makes sense.

2. Gravitational constant

The Friedmann equations in the Jordan frame define an effective gravitational constant

$$G_{\text{eff}} = G_*/F = G_* A^2. \quad (30)$$

This constant, however, does not correspond to the gravitational constant effectively measured in a Cavendish experiment. The constant measured in this type of experiment is

$$G_{\text{cav}} = G_* A_0^2 (1 + \alpha_0^2) \quad (31)$$

where the first term, $G_* A_0^2$, corresponds to the exchange of a graviton while the second term, $G_* A_0^2 \alpha_0^2$, is related to the long range scalar force.

Assuming fixed particle masses, the time variation of the gravitational constant is bounded [47] by

$$\frac{1}{G_{\text{cav}}} \frac{dG_{\text{cav}}}{dt} = \sigma_0 H_0, \quad |\sigma_0| < 5.86 \times 10^{-2} h^{-1}. \quad (32)$$

Choosing the number of Einstein frame e -folds as a time variable,

$$p = -\ln(1 + z_*), \quad (33)$$

implies that

$$2\alpha_0 \left[1 + \frac{\beta_0}{1 + \alpha_0^2} - \frac{\sigma_0}{2} \right] \frac{d\varphi_*}{dp} \Big|_0 = \sigma_0. \quad (34)$$

Note that the limit $\beta = -(1 + \alpha^2)$ that corresponds to the so-called Barker theory [48] in which $A = \cos \varphi_*$ leads to $\sigma = 0$ whatever the value of α and φ'_* so that the gravitational constant is strictly constant even though gravity is not described by general relativity.

D. Numerical implementation

The nuclear reaction network takes its standard form in Jordan frame. To compute the light elements abundances during BBN, one only needs to know the expansion rate history, $H(z)$, from deep in the radiation era up to today. It is thus convenient to express the Hubble parameter in the Jordan frame in terms of the one in the Einstein frame, using Eq. (16), as

$$AH = [H_* + \alpha(\varphi_*)\psi_*] \quad (35)$$

where ψ_* is defined by Eq. (20). Eq. (35) can also be expressed in the simple form

$$AH = H_* \left[1 + \alpha(\varphi_*) \frac{d\varphi_*}{dp} \right]. \quad (36)$$

It follows that, in terms of the cosmic time t , the equations of evolution can be recast as

$$\frac{d\varphi_*}{dt} = A^{-1}(\varphi_*)\psi_* \quad (37)$$

$$\frac{d\psi_*}{dt} = -A^{-1}(\varphi_*) \left[3H_*\psi_* + 4\pi G_*\alpha(\varphi_*)A^4(\varphi_*) \sum_i (1-3w_i)\rho_i + \frac{dV}{d\varphi_*} \right] \quad (38)$$

$$H_*^2 = \frac{8\pi G_*}{3} A^4(\varphi_*) \sum_i \rho_i + \frac{1}{3}\psi_*^2 + \frac{2}{3}V(\varphi_*) - \frac{K}{R_*^2} \quad (39)$$

$$\rho_i = \rho_{i0}(1+z)^{3(1+w_i)} \quad (40)$$

$$H = A^{-1} [H_* + \alpha(\varphi_*)\psi_*]. \quad (41)$$

The numerical integration is performed as follows. First we choose some initial value $\varphi_{\text{in}*}$, $\psi_{\text{in}*} = 0$ deep in the radiation era (typically, $z_{\text{in}} = 10^{12}$ and we integrate the system (37-41) to $z = 0$. We perform a shooting method so that the solution reaches the value $\Omega_{\Lambda 0}$ and G_N today, which fixes G_* and the energy scale of the potential. At this stage the value of φ_{*0} and α_0 are known. We also keep track of ψ_{0*} to infer the time variation of the gravitational constant, G_{cav} , and check its compatibility with the constraint (32). Subsequently, we perform a second integration of the same system including the nuclear reaction network.

III. MASSLESS DILATON WITH QUADRATIC COUPLING

The simplest model to consider consists of a massless dilaton with a quadratic coupling to matter. That is,

$$V(\varphi_*) = 0, \quad A = e^{a(\varphi_*)}, \quad a(\varphi_*) = \frac{1}{2}\beta\varphi_*^2. \quad (42)$$

It follows that

$$\alpha_0 = \beta\varphi_{0*}, \quad \beta_0 = \beta. \quad (43)$$

This model has been studied in detail in the literature, both in terms of its dynamics [8, 9] and of its BBN predictions [35, 36]. We use it as a test model to check our numerical scheme. In particular, the analytical behaviour of the field during the radiation and matter eras after BBN was obtained for a flat universe without cosmological constant in Ref. [35]. The numerical integration through BBN was also matched to this solution. Since we would like to use the same integration scheme for any potential and coupling, we can not rely on a particular analytic solution. It is used in this particular case only to check the accuracy of our code.

A. General study

As long as $V = 0$, the Klein-Gordon equation (21) can be rewritten in terms of the variable p defined by Eq. (33)

as

$$\frac{2}{3-\varphi_*'^2}\varphi_*'' + (1-w)\varphi_*' = -\alpha(\varphi_*)(1-3w). \quad (44)$$

As emphasized in Ref. [8], this is the equation of motion of a point particle with a velocity dependent inertial mass, $m(\varphi_*) = 2/(3-\varphi_*'^2)$, evolving in a potential $\alpha(\varphi_*)(1-3w)$ and subject to a damping force, $-(1-w)\varphi_*'$. During the cosmological evolution the field is driven toward the minimum of the coupling function. If $\beta > 0$, it drives φ_* toward 0, that is $\alpha \rightarrow 0$, so that the scalar-tensor theory becomes closer and closer to general relativity. When $\beta < 0$, the theory is driven away from general relativity and is likely to be incompatible with local tests unless φ_* was initially arbitrarily close to 0. Thus, we will restrict our analysis to $\beta > 0$.

We need to consider three regimes : (i) deep in the radiation era, (ii) the effect of particle annihilation during the radiation era (electron-positron annihilation in particular) and (iii) the transition between the radiation and matter era.

1. Deep radiation era

Deep in the radiation era, $w = 1/3$ and the coupling to φ_* is not efficient. The equation of evolution reduces to

$$\frac{2}{3-\varphi_*'^2}\varphi_*'' + \frac{2}{3}\varphi_*' = 0. \quad (45)$$

This can be integrated to give

$$\varphi_* = \varphi_{*i} - \sqrt{3} \ln \left[\frac{\alpha_i e^{-(p-p_i)} + \sqrt{1+\alpha_i^2} e^{-2(p-p_i)}}{\alpha_i + \sqrt{1+\alpha_i^2}} \right] \quad (46)$$

where α_i is defined by

$$\alpha_i = \frac{\varphi_{*i}'}{\sqrt{3-\varphi_{*i}'^2}} \quad (47)$$

and where φ_{*i} and φ_{*i}' are the values of φ_{*i} and its p -derivative at the initial time p_i . From Eq. (3), φ_* is expressed in Planck units and we will allow values of φ_{*i} to be of order unity. Interestingly, we see that in the radiation dominated era, φ_* rapidly tends to a constant value. The field derivative is just

$$\varphi_*' = \sqrt{\frac{3}{1+\alpha_i^2}} \alpha_i e^{-(p-p_i)} \quad (48)$$

so that it is divided by e^n in $\Delta p = n$ e-folds. In particular if we send $p_i \rightarrow -\infty$ then its variation between p_i and some time in the radiation era is

$$\Delta\varphi_* \rightarrow -\sqrt{3} \ln \left(\alpha_i + \sqrt{1+\alpha_i^2} \right). \quad (49)$$

It follows that, as long as $\varphi'_{*i} \ll \sqrt{3}$, $|\Delta\varphi_*| \sim \varphi'_{*i}$ and the field gets frozen at a constant value during radiation era. These properties can be recovered easily from the form of Eq. (21) of the evolution equation since it implies that $\dot{\varphi}_*$ decreases as R_*^{-3} . This behavior is quite general for dilaton-like fields [49]. In conclusion, deep in the radiation era (much before nucleosynthesis) the initial condition can be chosen to be $\dot{\varphi}_{*in} = 0$ and $\varphi_{*in} = \text{constant}$.

2. Mass thresholds

The previous analysis ignores an interesting effect [9] that appears when the universe cools below the mass of some species χ , $T \sim m_\chi$. This species becomes non-relativistic and induces a non-vanishing contribution to the r.h.s. of Eq. (21). For example, during electron-positron annihilation, the r.h.s. of Eq. (21) depends on $\Sigma_e = (\rho_e - 3P_e)/\rho_{\text{rad}}$.

In the Jordan frame the total energy density of the radiation is

$$\rho_{\text{rad}} = g_*(T) \frac{\pi^2}{30} T^4 \quad (50)$$

where g_* is the effective number of relativistic degrees of freedom,

$$g_*(T) = \frac{7}{8} \sum_{\text{fermion}} g_i + \sum_{\text{bosons}} g_i, \quad (51)$$

and T is the Jordan frame temperature of the radiation, as long as the particles are in thermal equilibrium with the radiation bath. The term $\rho_e - 3P_e$ takes the form [50]

$$\rho_e - 3P_e = \frac{g_e m_e^2}{2\pi^2} \int_0^\infty \frac{q^2}{e^{E/T} + 1} \frac{dq}{\sqrt{q^2 + m_e^2}}. \quad (52)$$

Introducing $x \equiv E/T$ and $z_e \equiv m_e/T$, we deduce that

$$\Sigma_e(T) = \frac{15}{\pi^4} \frac{g_e}{g_*(T)} z_e^2 \int_{z_e}^\infty \frac{\sqrt{x^2 - z_e^2}}{e^x + 1} dx \quad (53)$$

so that the Klein-Gordon equation (44) takes the form

$$\frac{2}{3 - \varphi_*'^2} \varphi_*'' + \frac{2}{3} \varphi_*' + \Sigma_e(T) \beta \varphi_* = 0. \quad (54)$$

The force term depends on the temperature which depends on $A(\varphi_*)$ and p . When this term is no longer effective, the field evolves according to Eq. (45) and tends to another constant, φ_{*out} . The relation between φ_{*in} and φ_{*out} , or equivalently between $a_{in} = a(\varphi_{*in})$ and a_{out} , has a complicated structure. Eq. (44) is almost a damped oscillator (because of the non-linear term). When $\Sigma_e(T) \beta \varphi_{*in}$ is small, the field does not have the time to oscillate while Σ_e is non-negligible, and the relation a_{in} - a_{out} is linear. For larger values of β and/or a_{in} one gets damped oscillations so that $a_{out} < a_{in}$. Figure 1 depicts the relation a_{in} - a_{out} for various values of the parameter β and Figure 2 illustrates the complexity of the full solution of this equation.

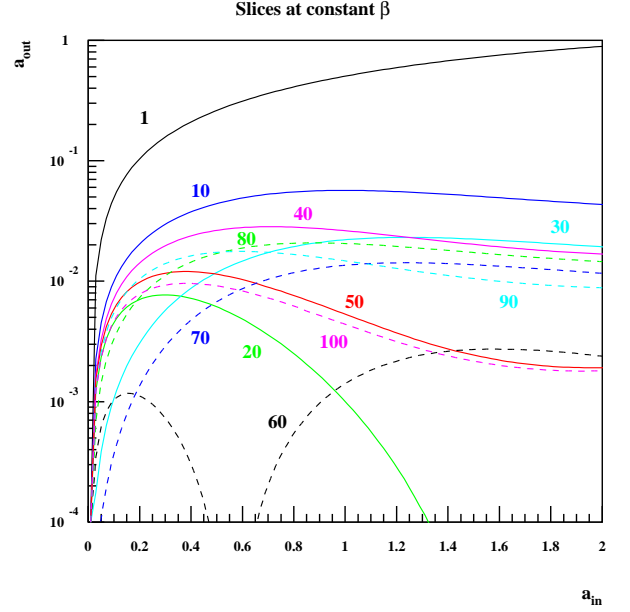


FIG. 1: a_{out} as a function of a_{in} for different values of β between 1 and 100. We see that $a_{out} < a_{in}$ which reflects the attraction towards general relativity during electron-positron annihilation.

3. Details of the field dynamics near threshold

Let us now investigate the dynamics of the attraction toward GR during a mass threshold in more detail. In general, the temperature is related to the integration variable p by

$$T[\varphi_*, p] = T_0 \frac{A_0}{A(\varphi_*)} \left[\frac{q_\gamma(T_0)}{q_\gamma(T)} \right]^{1/3} e^{-p} \quad (55)$$

where q_γ is the effective number of relativistic particles entering the definition of the entropy, taking into account *only* particles in equilibrium with the photons.

The dependence $T[\varphi_*, p]$ and the non-linear term $\varphi_*'^2/3$ make Eq. (54) difficult to integrate. In regimes where β and φ_{*in} are not too large then it can safely be approximated by

$$\varphi_*'' + \varphi_*' + \frac{3}{2} \Sigma_e(e^p) \beta \varphi_* = 0. \quad (56)$$

This approximate equation assumes that the field is slow rolling and that $A(\varphi_*)$ does not vary much during the transition. It is a linear equation in φ_* so that its solution is proportional to φ_{*in} .

Fig. 3 compares the solutions of the two equations (approximate and exact) for a single mass threshold. Indeed as long as β is small, the field is slow rolling and A remains almost constant during the transition. This is seen in the top panel of Fig. 3 for $\beta = 1$ and the field evolves to $\varphi_* \approx 0.84 \varphi_{*in}$. However when β is large and as a consequence $A(\varphi_{*in})$ is also large, the variation of φ_* during

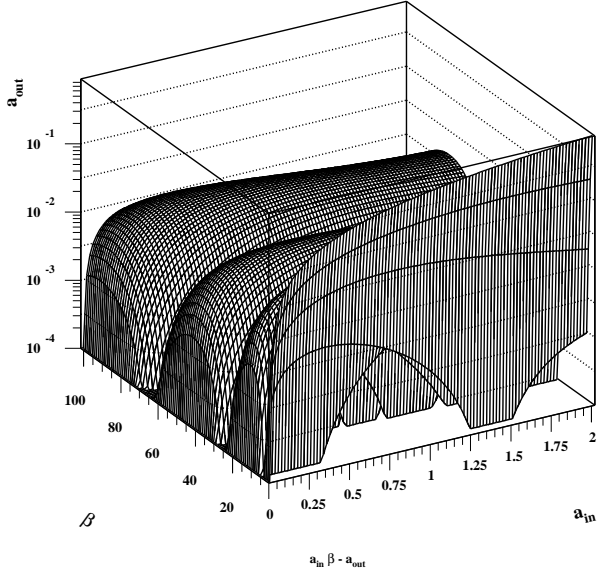


FIG. 2: The general structure of a_{out} as a function of a_{in} and β . This illustrates the complexity of the solutions of Eq. (44)

the transition implies, because of the relation (55) that a given width, ΔT , corresponds to a larger Δp , while this latter is fixed for the approximate solution. This implies that the attraction toward $\varphi_* = 0$ is more important. This progression is seen in the middle and lower panels of Fig. 3.

Fig. 4 compares the value $a_{\text{out}}/a_{\text{in}}$ as a function of β . When Eq. (56) is used, we recover the result of Ref. [9]. In this case, since this equation is linear, $a_{\text{out}}/a_{\text{in}}$ does not depend on the initial value of $\varphi_{*\text{in}}$ and is a universal function of β . This is compared to the ratio obtained from the integration of Eq. (54). As long as $\varphi_{*\text{in}}$ is small (typically of order 0.1), both results agree (because φ' remains small and A does not vary significantly). However, $a_{\text{out}}/a_{\text{in}}$ is typically 10 times smaller when $\varphi_{*\text{in}}$ is of order unity. This agrees with the results depicted in Fig. 1.

In conclusion, we see that both the dependence of the source term for φ_* and the non-linear term in φ'_* lead to significant modifications of the dynamics when the initial value of the scalar field or β are large.

4. Expected value of a_{in}

In the previous analysis we have restricted ourselves to a_{in} between 0 and 3, mainly for numerical reasons. We can now be in a position to justify this choice. Indeed, and as noted earlier, because the scalar field is frozen during the radiation dominated era, we need only specify $\varphi_{*\text{in}}$ as an initial condition. For a given value of β , this fixes

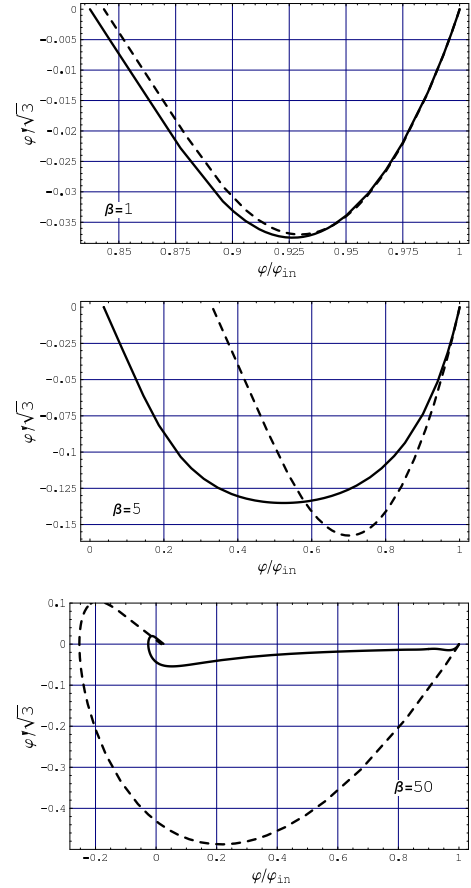


FIG. 3: Evolution of the scalar field in phase space during a transition for $\beta = 1, 5, 50$ from top to bottom when we assume $\varphi_{*\text{in}} = 1$. The solid line corresponds to the exact solution of Eq. (54) while the dashed line corresponds to the solution of the approximate equation (56).

the initial value of a_{in} .

It is difficult to predict the value of a_{in} from general arguments. For instance, if we expect $\varphi_* \sim 1$ (in Planck units) at the end of inflation, this means that $\alpha_{\text{in}} \sim \beta$ and $a_{\text{in}} \sim \beta/2$. In this case, one would indeed like to investigate a_{in} with values up to roughly 50. On the other hand, if we expect a deviation from general relativity of order one at the end of inflation, then we might expect $\alpha_{\text{in}} \sim 1$, or $\varphi_* \sim \beta^{-1}$ and $a_{\text{in}} \sim \beta^{-1}/2$. In that latter case restricting to $a_{\text{in}} \sim 3$ would be safe. Clearly, without a detailed model of the inflationary period it is difficult to determine the “natural” range of variation of a_{in} .

To get some insight on the expected order of magnitude of a_{in} just before the period of electron-positron annihilations, we must investigate the effect of higher mass thresholds. To that end, we consider an extension of Eq. (54) in which the source term is replaced by a sum

$$\Sigma(T) = \sum_{\text{species}} \Sigma_i(T), \quad (57)$$

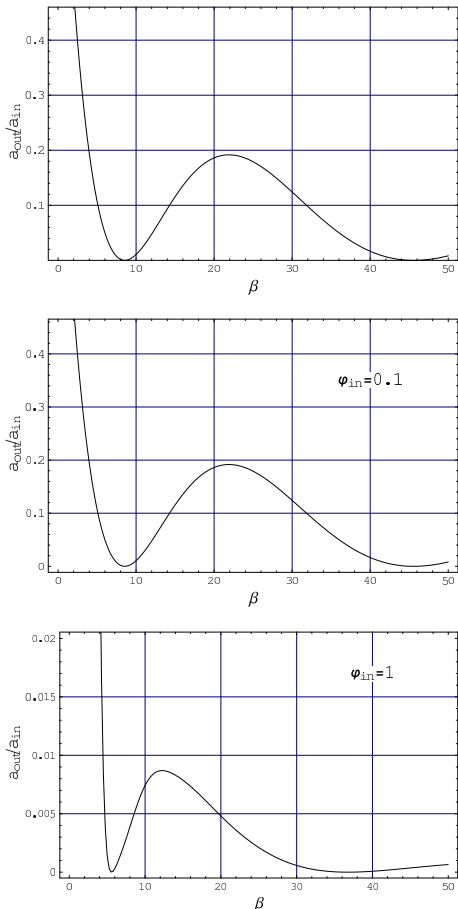


FIG. 4: Evolution of $a_{\text{out}}/a_{\text{in}}$ as a function of β . (Top): when we used the approximate equation (56), it does not depend on the initial value of the scalar field, $\varphi_{*\text{in}}$. (middle and bottom): we use the exact equation (54). This equation being non-linear the ratio depends on the initial value of $\varphi_{*\text{in}}$.

where

$$\Sigma_i(T) = \frac{15}{\pi^4} \frac{g_i}{g_*(T)} z_i^2 \int_{z_i}^{\infty} \frac{\sqrt{x^2 - z_i^2}}{e^x + \epsilon} dx \quad (58)$$

with $z_i = m_i/T$, $\epsilon = +1$ for fermions and $\epsilon = -1$ for bosons.

In principle, all massive standard model particles will play a role. In addition to electrons and positrons, we must consider the effects of muons, pions, charmed quarks, taus, bottom quarks, W^\pm bosons, Z^0 boson and the top quarks. The role of lighter quarks is tied to the quark hadron transition whose effect we do not include. Nor do we include the effect of the Higgs boson due to its as yet uncertain mass. Fig. 5 depicts the evolution of Σ with (the Jordan frame) temperature. In particular, it shows that the effects of the various thresholds cannot be considered separately because the transitions overlap and the scalar field, φ_* , does not have time to settle back to $\varphi'_* = 0$ between two transitions. Also note that, fortunately, the last threshold (electron-positron annihilation)

is almost decoupled from the previous ones. Thus, we will be able to compute the state of the scalar field just before the last transition which is of primary importance for BBN.

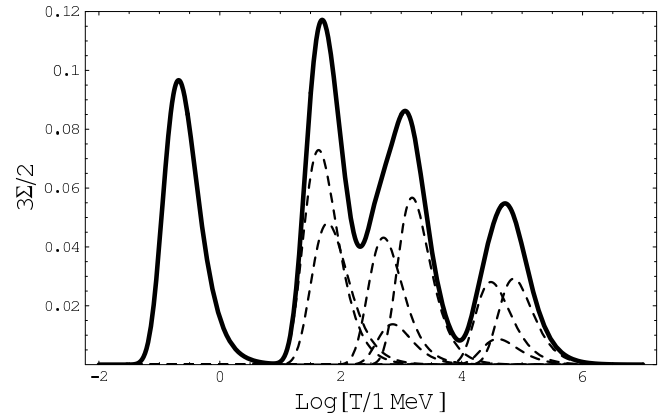


FIG. 5: The source function, $\Sigma(T)$, entering the Klein-Gordon equation when the mass thresholds corresponding to the particles listed in the text. The dashed curves show the individual particle contributions, $\Sigma_i(T)$, and the solid curve shows the sum, $\Sigma(T)$.

Fig. 6 describes the dynamics of this multi-threshold phase (including the electron-positron annihilation). As long as β or $\varphi_{*\text{in}}$ remain small, we see that each of the four peaks of Σ , corresponds to a well defined departure from $\varphi'_* = 0$ with movement towards smaller φ_* proportional to the initial value $\varphi_{*\text{in}}$. For larger values, the field is first slow-rolling and then oscillates around $\varphi_* = 0$. In this case, we see that the effect of the four peaks cannot be considered separately because the field does not have time to settle back to $\varphi'_* = 0$ between two transitions.

The evolution of φ_* , when mass thresholds are non-negligible, allows us to determine the value of a_{in} prior to the period of electron-positron annihilation. We denote this value by a_{ee} . Fig. 7 shows $a_{\text{ee}}/a_{\text{in}}$, that is the value of $a(\varphi_*)$ just before electron-positron annihilation compared to its initial value at very high temperature, as a function of β . The attraction toward general relativity is very drastic. In the case where $\varphi_{*\text{in}}$ is of order unity, we conclude that $a_{\text{ee}} \lesssim 10^{-4} \times a_{\text{in}} \sim 10^{-4} \beta/2 \lesssim 5 \times 10^{-3}$. It follows that restricting to $a_{\text{in}} = 0-3$ at before electron-annihilation is a safe limit even if $\varphi_* \sim \mathcal{O}(1)$ at the end of the inflationary phase.

Note also that phase transitions are another source of attraction toward general relativity. We have not included either the quark-hadron transition or the electroweak transition in the previous analysis. During a phase transition, there is generally a significant modification of the equation of state which will induce a source term in the Klein-Gordon equation.

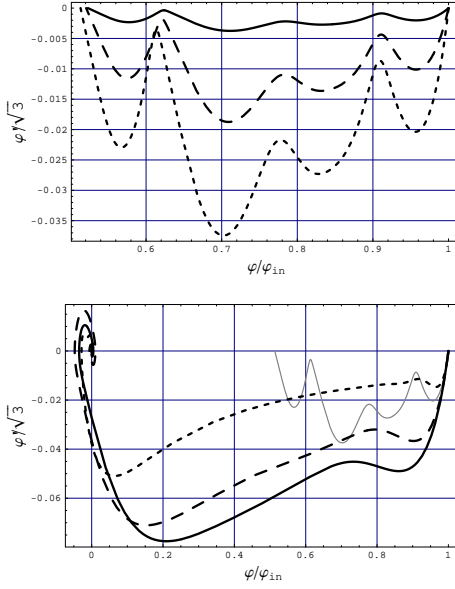


FIG. 6: Dynamical evolution of φ_* when the source term is described by Fig. 5. (Top) we have set $\beta = 1$ and $\varphi_{*in} = 0.1, 0.5, 1$ (solid, dashed, dotted). (Bottom) We have fixed $\varphi_{*in} = 1$ and taken $\beta = 1, 15, 20, 50$ (thin solid, solid, dashed, dotted).

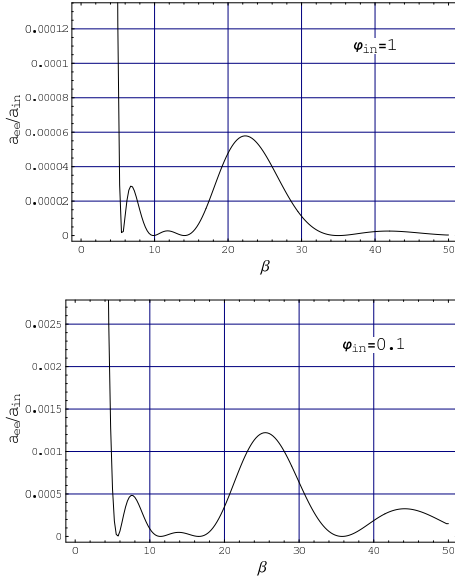


FIG. 7: Evolution of a_{ee}/a_{in} as a function of β when the source term is described by Fig. 5 just before the electron-positron annihilation. (Top): $\beta = 1$ (Bottom): $\beta = 0.1$.

5. Radiation-matter transition

In principle, BBN will place a constraint on the value of a_{out} . As such, our constraint will in effect be dependent on a_{in} which is unknown. To compare these constraints to the ones obtained in the Solar system, we need to relate

a_{out} to a_0 . We allow the code to integrate the evolution equation up to the present, so that we obtain a_0 directly.

For the particular case of a vanishing potential or as long as the field is slow rolling, $\varphi' \ll 1$, one can approximate $3 - \varphi_*'^2 \sim 3$ so that Eq. (44) takes the simplified form

$$y(y+1)\frac{d^2\varphi_*}{dy^2} + \frac{1}{2}(5y+4)\frac{d\varphi_*}{dy} + \frac{3}{2}\beta\varphi_* = 0, \quad (59)$$

where we have introduced the variable $y \equiv R_*/R_{dec*}$ and used the fact that the gas is a mixture of pressureless matter and radiation and the equation of state is $w = 1/3(1+y)$. This equation allows us to relate the value of the scalar field deep in the radiation era but after BBN, φ_{out*} , to its value today, φ_{0*} . Its solution is a hypergeometric function, $f_\beta(y) = {}_2F_1[s, s^*, 2; -y]$ with $s = 3/4 - i\sqrt{3(\beta - 3/8)}/2$ so that

$$\varphi_{0*} = \varphi_{out*} f_\beta(y_0) \quad (60)$$

where the matching to the analytical solution has been performed after the end of nucleosynthesis at a time where φ_* is constant. y_0 is given by

$$y_0 = \frac{R_0}{R_{dec}} \frac{A_{eq}}{A_0} = (1 + z_{eq}) \exp[(\alpha_{eq}^2 - \alpha_0^2)/2\beta]. \quad (61)$$

This method avoids integrating the system (37-41) to the present but requires a determination of y_0 . Indeed when φ has not varied significantly between BBN and equality, then

$$y_0 \simeq (1 + z_{eq}) \exp[(\alpha_{out}^2 - \alpha_0^2)/2\beta]. \quad (62)$$

However, this solution cannot be generalized to a Λ -CDM or to extended quintessence models. For this reason we do not use this method and integrate the system numerically from z_{in} to $z = 0$. Figure 8 compares our numerical integration, from which we determine the exact value of y_0 and the analytic solution (60). We see that the agreement is almost perfect. It can be checked that an error smaller than 10% on the evaluation of y_0 left a_0 almost unchanged. Let us emphasize that in more general cases, i.e. for different potentials and coupling functions, such an analytic solution is in general not known so that the full numerical approach is necessary.

The solution (60) implies that $\varphi_{*0}' = \varphi_{out} g_\beta(y_0)$ with $g_\beta(y_0) = -3\beta y_0 {}_2F_1(1 + s, 1 + s^*, 3; -y_0)/4$. It is then possible to estimate, from Eq. (32), the value of σ_0 as a function of (α_{out}, β) ,

$$\sigma_0 = 2\alpha_{out} g_\beta(y_0) \frac{1 + \frac{\beta}{(1 + \alpha_{out}^2) f_\beta^2(y_0)}}{1 + \frac{\alpha_{out}^2}{\beta} f_\beta(y_0) g_\beta(y_0)}. \quad (63)$$

As shown by Fig. 9, as soon as $\alpha_{out} \lesssim 1$, the constraint on σ_0 is satisfied. This means that for the quadratic coupling model, nearly all parameter choices satisfy this constraint.

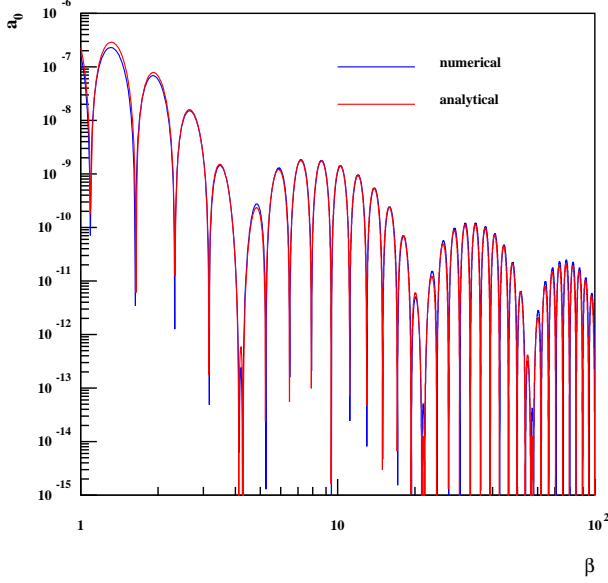


FIG. 8: Comparison of the numerical integration and the analytical solution for a flat CDM model with $a_{\text{in}} = 1$.

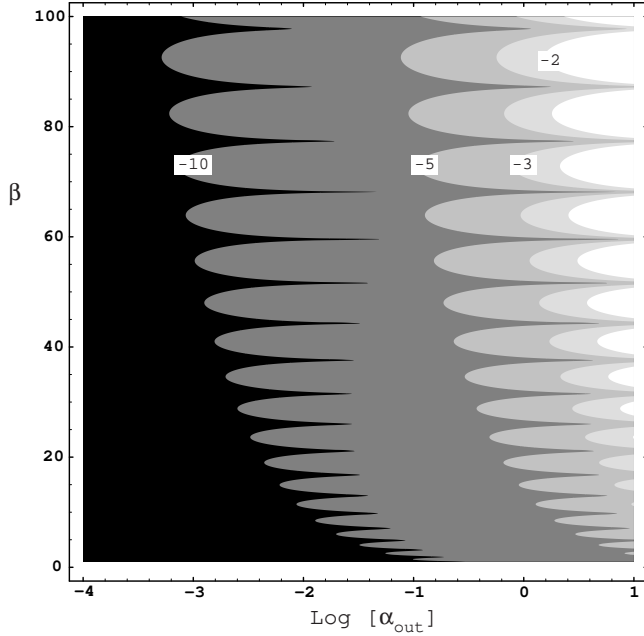


FIG. 9: σ_0 as a function of α_{out} and β . The labels on the contour lines give the value of $\log |\sigma_0|$.

The constraint on σ_0 leading to $a_{\text{out}} < 1$ is an *a posteriori* argument for not considering very large values of a_{in} at electron-positron annihilation. Very large values of a_{in} will in general lead to large values of a_{out} that are constrained by local tests on the constancy of the gravitational constant.

6. Equivalent speed-up factor

As long as $V = 0$ and one can neglect the curvature term, the Friedmann equation (18) can be written, using Eq. (35) as

$$3 \frac{1 - \varphi'^2/3}{(1 + \alpha\varphi_*')^2} H^2 = 8\pi G_* \rho A^2. \quad (64)$$

Comparing this to the standard Friedmann equation, $3H_{GR}^2 = 8\pi G_* A_0^2 (1 + \alpha_0^2) \rho$, one obtains the speed-up factor defined to be the ratio of the Hubble parameters,

$$\xi = \frac{A(\varphi_*)}{A_0} \frac{1 + \alpha(\varphi_*)\varphi_*'}{\sqrt{1 - \varphi'^2/3}} \frac{1}{\sqrt{1 + \alpha_0^2}}. \quad (65)$$

Figure 10 shows the variation of the speed-up factor during BBN for various values of β , taking into account the effects of electron-positron annihilation. ξ is constant above $z \sim 2 \times 10^{11}$ and below $z \sim 10^9$. For large values of β , typically $\beta \gtrsim 5$, the attraction toward general relativity is so efficient that $\xi \sim 1$ for $z \lesssim 10^9$. For smaller values, ξ is frozen at some constant value $\xi > 1$ at the end of BBN and will be driven towards 1 only when the subsequent evolution due to matter domination will be significant. For very small values of β , as pointed out in Ref. [35] and as we have shown earlier, φ_* is almost constant during the electron-positron annihilation period. As a result, $\varphi_{*\text{out}} = \varphi_{*\text{in}}$ and $\varphi_*' \sim 0$ so that

$$2 \ln \xi = \beta^{-1} (\alpha_{\text{in}}^2 - \alpha_{\text{out}}^2) - \ln(1 + \alpha_0^2). \quad (66)$$

In a more complex situation, one cannot approximate this factor by a constant and the full dynamics during BBN must be determined. In particular, we see that ξ drops around the time the neutron-to-proton ratio, n/p , freezes out, but generically reaches a constant value during the nucleosynthesis period.

More tuned models in which the variation of ξ is not finished during BBN may lead to some signatures on the primordial abundances (see e.g. [51] for a proposal). Indeed, no model independent statements can be made but in general we expect them to be very constrained, in particular if the mass thresholds prior to electron-positron annihilation are taken into account. Such models can easily be discussed in future works with the tool presented here.

B. Numerical simulations

The time evolution of $a(\varphi_*)$ is depicted in Figure 11 for three values of β . It is obtained by numerically integrating the equations of § IID by a standard Runge-Kutta method. In the top panel of Figure 11. The two plateaus at high z correspond to the constant values of a during the radiation era before and after BBN. Oscillatory behaviour due to the damped oscillation of the

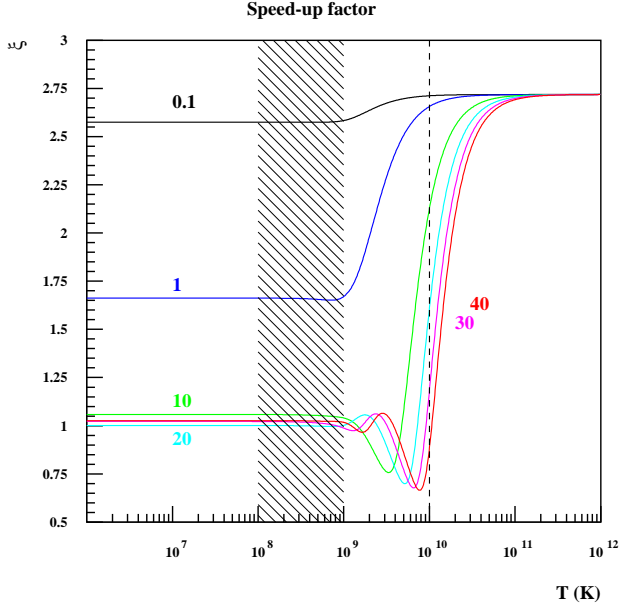


FIG. 10: Variation of the speed-up factor during BBN for various values of β starting from the same value of a_{in} . For small values of β , ξ is almost constant and is driven toward 1 during the subsequent matter dominated era. For example, for $\beta \lesssim 0.2$ ξ is constant during BBN. For larger values of β , the attraction toward general relativity is very efficient and $\xi \sim 1$ during BBN. The dashed line represents the time of n/p freeze-out and we have indicated the interval during which light elements are formed.

field, as described by Eq. (60) begins when the matter density becomes comparable to the radiation density. In this case, we find that $a_{\text{out}} \approx 0.05$ and $a_0 \approx 10^{-9}$. This implies that $\alpha_0 \approx 1.4 \times 10^{-4}$. In addition, $d\phi_*/dp|_0 = \psi_*/H_* \approx 2 \times 10^{-5}$ leading to $\sigma_0 \approx 7 \times 10^{-8}$, easily satisfying the post-Newtonian constraints discussed above. For the other examples depicted in Fig. 11, we have $a_{\text{out}} = 1.3 \times 10^{-3}$, $a_0 = 2.7 \times 10^{-12}$, $\alpha_0 \approx -2 \times 10^{-5}$, $\psi_*/H_* \approx 4 \times 10^{-7}$, and $\sigma_0 \approx -9 \times 10^{-10}$ ($\beta = 60$) and $a_{\text{out}} = 0.5$, $a_0 = 1.7 \times 10^{-7}$, $\alpha_0 \approx 6 \times 10^{-4}$, $\psi_*/H_* \approx -1 \times 10^{-3}$, and $\sigma_0 \approx -3 \times 10^{-6}$ ($\beta = 1$).

In the middle panel of Figure 11, we show the evolution of a for $\beta = 60$. As expected, the larger coupling allows for several oscillations during e^+e^- annihilation, and significantly more oscillations during the matter dominated era. The dashed line shows the redshift corresponding to matter-radiation equality. We see that the field starts oscillating before equality due to the enhanced coupling. Comparing the two panels, we see that as β increases oscillations begin at higher redshift.

C. BBN calculations

The equations displayed in section IID have been implemented in our BBN code [27, 28]. The source term

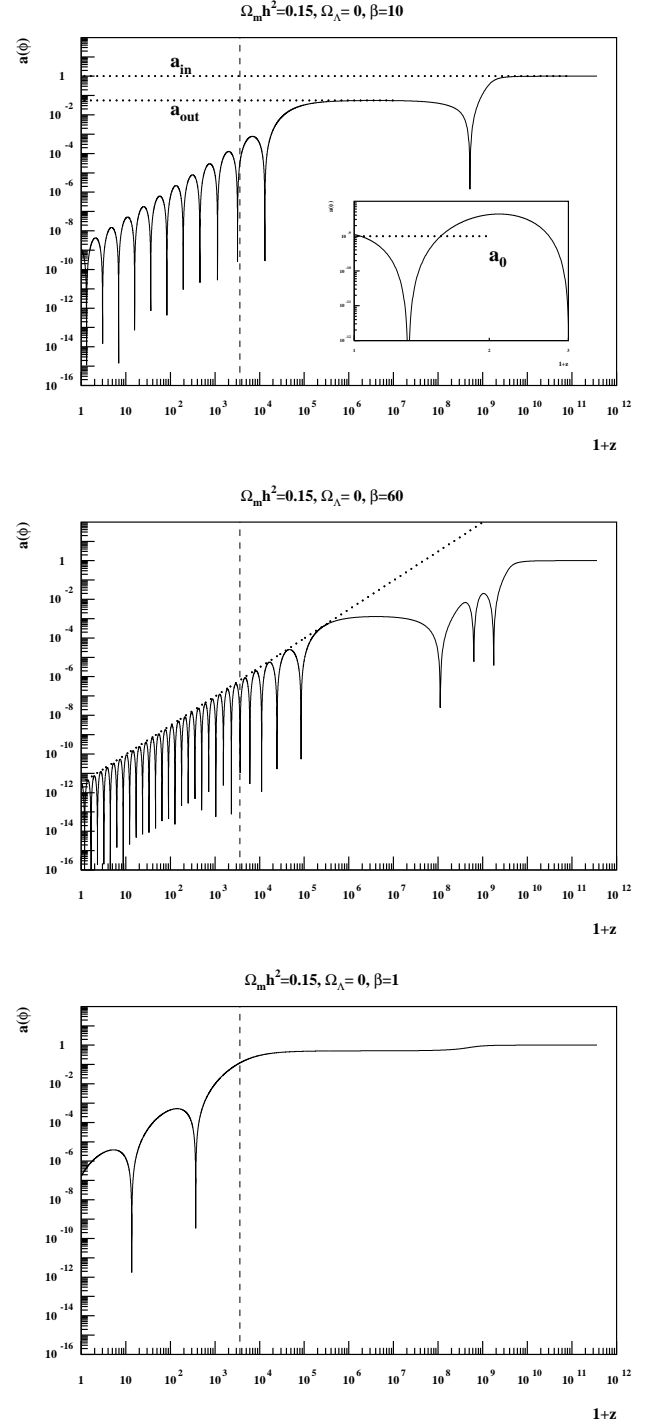


FIG. 11: $a(\phi_*)$ as a function of z for $\beta = 10$ (top), $\beta = 60$ (middle) and $\beta = 1$ (bottom) assuming $a_{\text{in}} = 1$. The dashed lines show the redshift corresponding to matter-radiation equality. In the top panel, the dotted lines define a_{in} , a_{out} and a_0 while in the middle panel it emphasizes the $(1+z)^{3/2}$ overall dependence of $a(\varphi)$.

due to the electron-positron contribution to the energy and entropy density is calculated by a numerical integration of the fermi distributions. The calculation starts at $T=10^{12}$ K well above electron-positron annihilations and weak interaction freeze-out with a given value of β , a_{in} and $d\varphi_*/dt_*=0$. For a given value of $\Omega_b h^2$, a grid of calculations is performed with a_{in} ranging from 0. to 3. in steps of 10^{-3} and β ranging from 0.1 to 100. in steps of 0.1 ($\beta < 10$) and 1. ($\beta > 10$). Let us emphasize that the range in a_{in} is conservative given the analysis of the previous section. Small steps are needed because of the complicated structure displayed in Fig. 2. The ${}^4\text{He}$ and D yields are compared to the allowed intervals, discussed in the next section, and for each β value, the maximum allowed value of a_{out} is determined and the numerical calculation is extended to obtain the present limits on a_0 and α_0 . (The minimum allowed a_{out} value was found to be zero in all considered cases.) However, because of the late domination of matter, the limits on a_0 display many more oscillations than the limits on a_{out} as a function of β . Hence, steps 100 times smaller in β were used for the calculation of a_0 using interpolated values of the relatively slowly varying a_{out} .

Figures 12 to 17 illustrate the dependence of D, ${}^4\text{He}$ and ${}^7\text{Li}$ in terms of the baryon-to-photon ratio, $\eta = \eta_{10} \times 10^{-10}$, the parameter β and the initial condition of the field, a_{in} for a model with quadratic coupling and vanishing potential. It is evident that the D mass fraction is only very weakly affected by the two new parameters (β, a_{in}). ${}^7\text{Li}$ is also almost independent of a_{in} but the valley around $\log(\eta_{10}) = 0.5$ becomes deeper as β increases. The most sensitive of the light elements is ${}^4\text{He}$. Its abundance depends strongly on both parameters. This reflects the fact that the expansion rate of the universe is modified by this scalar-tensor theory of gravity.

D. Constraints on primordial abundances

A comparison of the previous set of computations with the observational determination of the light element abundances will allow us to set constraints on this class of models. The abundance data are obtained from spectroscopic observations and compared directly with BBN predictions assuming the WMAP determination of Ω_b [26, 27, 28, 29, 30]. We now discuss these observations.

1. D/H

The best determinations of primordial D/H are based on high-resolution spectra in high-redshift, low-metallicity quasar absorption systems (QAS), via its isotope-shifted Lyman- α absorption. The five most precise observations of deuterium [52, 53, 54, 55] in QAS give $\text{D/H} = (2.78 \pm 0.29) \times 10^{-5}$, where the error is statistical only.

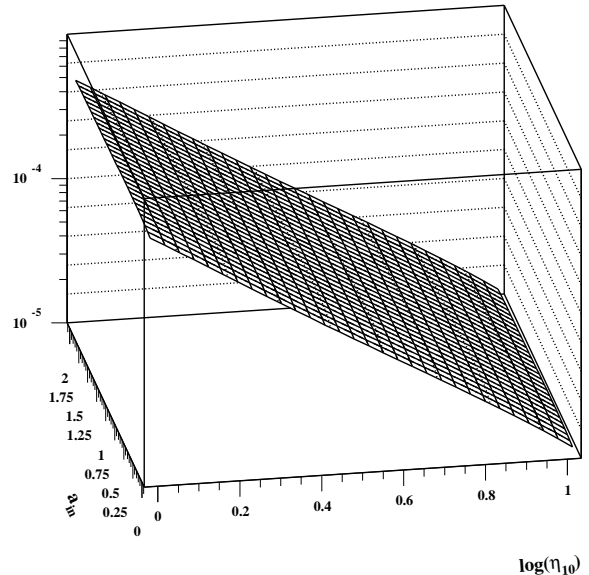


FIG. 12: D mass fraction as a function of the baryonic density ($\log(\eta_{10})$) and a_{in} for $\beta = 20$. The abundance of D is almost insensitive to a_{in} .

Using the WMAP value for the baryon density [25] the primordial D/H abundance is predicted to be [27]:

$$(\text{D/H})_p = 2.60^{+0.19}_{-0.17} \times 10^{-5} \quad (67)$$

This value is in very good agreement with the observational one. Nevertheless, as we will see below, the agreement between predicted D/H abundance and observations is not very sensitive to the change the gravitational sector of the theory.

2. ${}^4\text{He}$

${}^4\text{He}$ is observed in clouds of ionized hydrogen (HII regions), the most metal-poor of which are in dwarf galaxies. There is now a large body of data on ${}^4\text{He}$ and CNO in these systems [56, 57] for which an extended data set including 89 HII regions obtained $Y_p = 0.2429 \pm 0.0009$ [57]. However, the recommended value is based on the much smaller subset of 7 HII regions, finding $Y_p = 0.2421 \pm 0.0021$.

It is important to note that ${}^4\text{He}$ abundance determinations depend on a number of physical parameters associated with the HII region in addition to the overall intensity of the He emission line. These include, the temperature, electron density, optical depth and degree of underlying absorption. A self-consistent analysis may use multiple ${}^4\text{He}$ emission lines to determine the He abundance, the electron density and the optical depth. The question of systematic uncertainties was addressed in some detail in [58]. It was shown that there exist severe de-

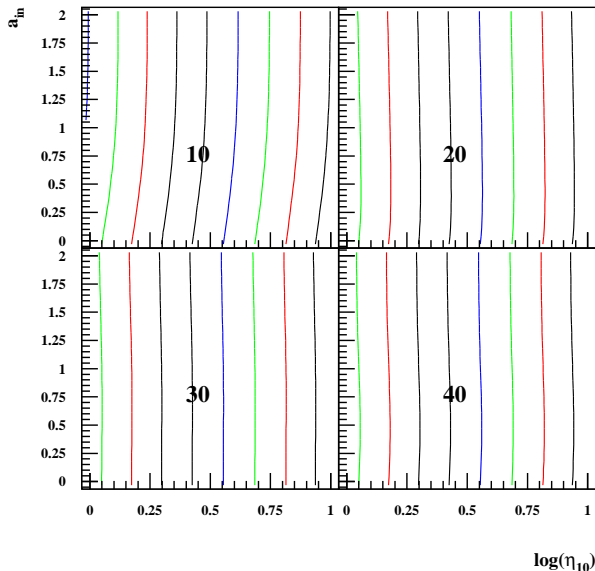


FIG. 13: Contour plots for D/H as function of a_{in} and η_{10} but for different values of β : 10, 20, 30 and 40. (For $\beta=20$, this is the same as Fig. 12.) The contours are evenly spaced by step of $\Delta \log(\text{D}/\text{H}) = 0.2$ starting from $\log(\text{D}/\text{H}) = -4.8$ on the right. We conclude that the dependence of D mass fraction on β is mild.

degeneracies inherent in the self-consistent method, particularly when the effects of underlying absorption are taken into account. These degeneracies are markedly apparent when the data is analyzed using Monte-Carlo methods which generate statistically viable representations of the observations. When this is done, not only are the He abundances found to be higher, but the uncertainties are also found to be significantly larger than in a direct self-consistent approach.

Recently a careful study of the systematic uncertainties in ^4He , particularly the role of underlying absorption has been performed [59] using a subset of the highest quality from the data of Izotov and Thuan [56]. All of the physical parameters listed above including the ^4He abundance were determined self-consistently with Monte Carlo methods. The extrapolated ^4He abundance was determined to be $Y_p = 0.2495 \pm 0.0092$ [59]. Conservatively, it would be difficult at this time to exclude any value of Y_p inside the range $0.232 - 0.258$.

At the WMAP value for η , the ^4He abundance is predicted to be [27]

$$Y_p = 0.2479 \pm 0.0004 \quad (68)$$

and it is in excellent agreement with the most recent analysis of the ^4He abundance [59]. As we will show, although ^4He remains the most discriminatory element for physics beyond the standard model, the current large uncertainty in its primordial value will impede tight constraints on the parameters used to extend minimal Einstein gravity.

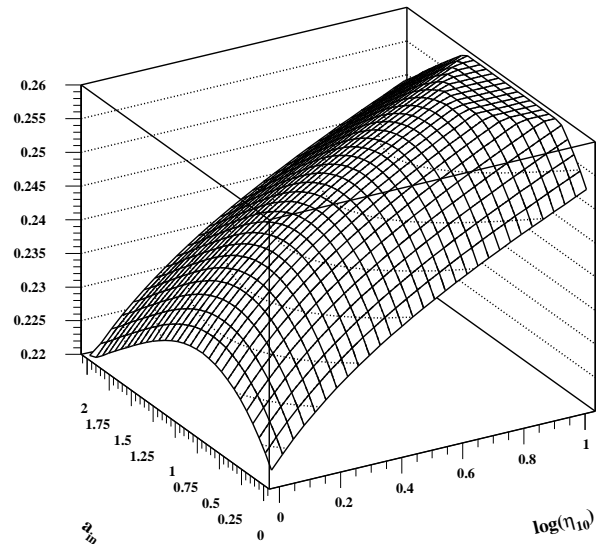


FIG. 14: As in Figure 12 but for ^4He . ^4He is the most sensitive element to the value of a_{in} .

3. $^7\text{Li}/\text{H}$

The systems best suited for Li observations are metal-poor halo stars in our Galaxy. Analyses of the abundances in these stars yields [60] $\text{Li}/\text{H}|_p = (1.23^{+0.34}_{-0.16}) \times 10^{-10}$.

The ^7Li abundance based on the WMAP baryon density is predicted to be [27]:

$$^7\text{Li}/\text{H} = 4.15^{+0.49}_{-0.45} \times 10^{-10} \quad (69)$$

This value is in clear contradiction with most estimates of the primordial Li abundance, as also shown by [30] who find :

$$^7\text{Li}/\text{H} = 4.26^{+0.73}_{-0.60} \times 10^{-10} \quad (70)$$

In both cases, the ^7Li abundance is a factor of ~ 3 higher than the value observed in most halo stars.

An important source for potential systematic uncertainty stems from the fact that the Li abundance is not directly observed but rather, inferred from an absorption line strength and a model stellar atmosphere. Its determination depends on a set of physical parameters and a model-dependent analysis of a stellar spectrum. Among these parameters, are the metallicity characterized by the iron abundance (though this is a small effect), the surface gravity which for hot stars can lead to an underestimate of up to 0.09 dex if $\log g$ is overestimated by 0.5, though this effect is negligible in cooler stars. The most important source for error is the surface temperature. Effective-temperature calibrations for stellar atmospheres can differ by up to 150–200 K, with higher

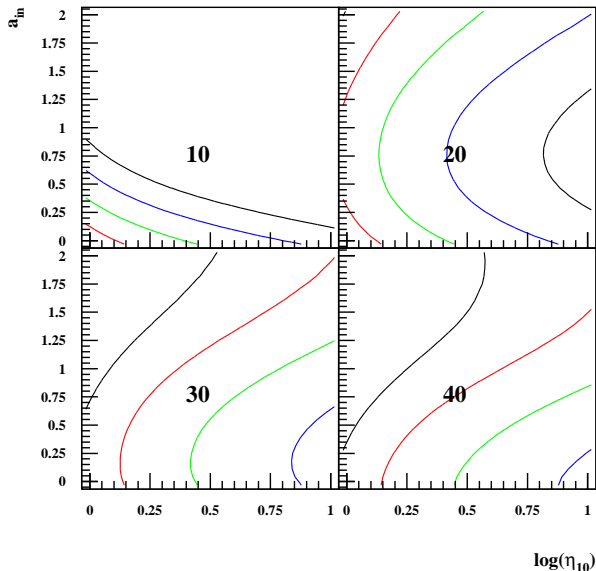


FIG. 15: As in Fig. 13 but for ${}^4\text{He}$. Contours correspond from left to right to $Y_p = 0.22, 0.23, 0.24, 0.25$ and 0.26 (i.e. black, red, green, blue and black respectively.) The abundance of ${}^4\text{He}$ is very sensitive to β . In addition, the dependence on a_{in} is increased for larger values of β .

temperatures resulting in estimated Li abundances which are higher by ~ 0.08 dex per 100 K. Thus accounting for a difference of 0.5 dex between BBN and the observations, would require a serious offset of the stellar parameters. We note that there has been a recent analysis [61] which does support higher temperatures, and brings the discrepancy between theory and observations to within 2σ .

We are now in a position to directly compare our numerical results for the BBN production of light elements in a scalar-tensor theory of gravity with observations. In Fig. 18, we show the resulting light element abundances as a function of a_{in} with $\Omega_b h^2 = 0.0224$ for values of β between 5, 10, 15, 20, 25, 30, 50, and 100. Starting with D/H, we see from Fig. 18 that D is always compatible with observation as long as $\beta \gtrsim 10$. For lower values both D and ${}^4\text{He}$ will set constraints. Of course for very small beta, we must have small values of a_{in} as we approach standard GR. In that case, the concordance of D/H is also restored. We must also emphasize that ${}^7\text{Li}$ cannot be reconciled with observation in this class of models.

Fig. 19 depicts the constraints expected on (a_{out}, β) . The black solid curve shows the maximum possible value of a_{out} for $a_{\text{in}} = 0 - 2$. We also show the maximum allowed value of a_{out} from BBN for two choices of $\Omega_b h^2 = 0.0224$ (solid) and 0.024 (dashed) based on ${}^4\text{He}$ (red) and D/H (blue). We see that for all β , ${}^4\text{He}$ always sets the tightest constraints. Interestingly for $\beta \gtrsim 20$, the attraction toward general relativity is so efficient that, assuming reasonable values for a_{in} , all abundances are

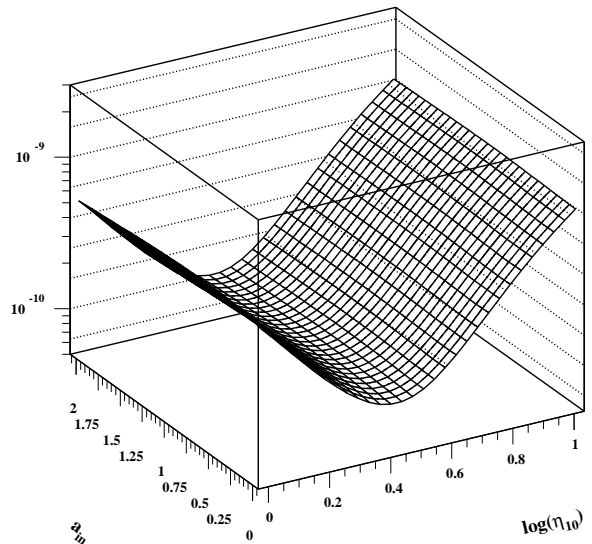


FIG. 16: As in Figure 12 but for ${}^7\text{Li}$. As in the case of deuterium, ${}^7\text{Li}$ depends very mildly on a_{in} .

compatible with observations.

E. Using WMAP to fix Ω_b

As we have seen from the previous discussion, one can set sharp constraints on the primordial abundances if $\Omega_b h^2$ is set by the analysis of the CMB anisotropies. It is important to note however, that the WMAP data has been analyzed in a standard cosmological set up which assumes general relativity, that is $\alpha = \beta = 0$. As was shown in Ref. [16], the CMB power spectrum in scalar-tensor theories is modified in 3 principle ways: (1): the modification of the Friedmann equations induces a change in the age of the universe and in the sound horizon thus shifting the acoustic peak structure, (2) the amplitude of Silk damping is modified because it depends on the photon diffusion length at recombination and thus on the Hubble size at this time, and (3) the thickness of the last scattering surface is modified. In any specific model, one needs to check to what extent the CMB angular power spectrum is modified and decide whether the constraints set by WMAP can be used as is or if one needs to go through a combined analysis to get new consistent constraints.

As was shown in Ref. [16], for the case of the quadratic coupling adopted here, CMB anisotropies are not affected by this modification to gravity and hence we can safely use WMAP data to fix the baryon density. But, in general, this will not be the case in other models (see e.g. Ref. [21]).

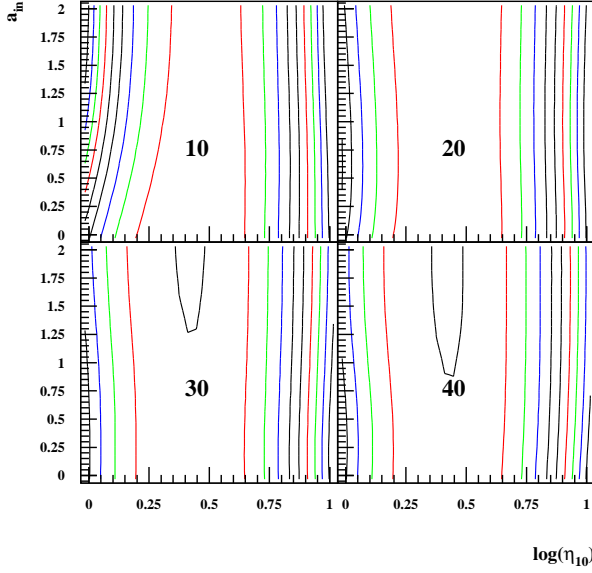


FIG. 17: As in Fig. 13 but for ${}^7\text{Li}$. The contours are evenly spaced by steps of $\Delta\text{Li}/\text{H}=1.10^{-10}$ starting from the value of $\text{Li}/\text{H}=1.10^{-10}$ (in black only seen in the lower diagrams). ${}^7\text{Li}$ shows little dependence on β except for values of $\log(\eta_{10})$ corresponding to the minimum value of ${}^7\text{Li}$.

IV. INCLUDING A COSMOLOGICAL CONSTANT

A. Generalities

The previous model does not account for the observed late acceleration of our universe. One can easily generalize it by introducing a cosmological constant. Let us however stress that there is no unique way to introduce such a constant in scalar-tensor theories.

One way to generalize the model is to introduce a cosmological constant in the Einstein frame which corresponds to a flat potential for the dilaton, so that the spin-0 degree of freedom remains massless. In this case, we consider models in which

$$V(\varphi_*) = V_0, \quad a(\varphi_*) = \frac{1}{2}\beta\varphi_*^2. \quad (71)$$

The energy density in the Jordan frame related to the constant V_0 is not a constant energy density and corresponds to a potential $U(\varphi) = 2V_0A^{-4} = 2V_0F^2(\varphi)$.

Alternatively, we can introduce a constant energy density in the Jordan frame. This amounts to choosing

$$V(\varphi_*) = U_0A^4(\varphi_*)/2, \quad a(\varphi_*) = \frac{1}{2}\beta\varphi_*^2. \quad (72)$$

The value of either V_0 or U_0 is set by the observed value of the cosmological constant density parameter today.

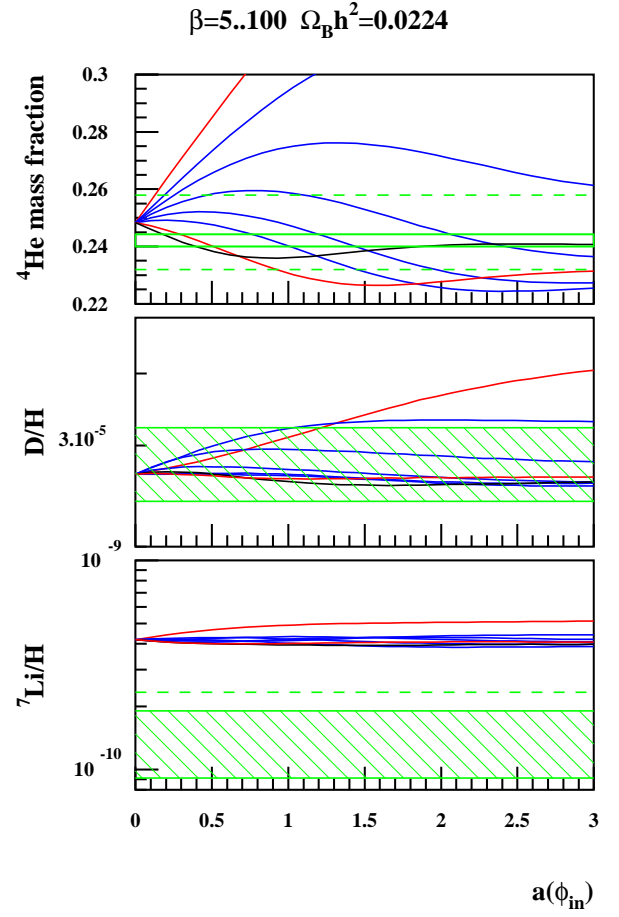


FIG. 18: ${}^4\text{He}$, D and ${}^7\text{Li}$ abundances as a function of a_{in} for $\beta = 5, 10, 15, 20, 25, 30, 50$, and 100 (The maximum deviations correspond to the lowest values of β). The baryonic density is set by WMAP observations and is assumed to be independent of the scalar component of gravity. For $\beta > 10$ D is always compatible with observations and will set no constraint while ${}^7\text{Li}$ cannot be reconciled with observations. We conclude that BBN constraints will mainly arise from ${}^4\text{He}$.

The properties of these models can be discussed by generalizing Eq. (44) when the potential does not vanish [12, 14]. As such, we set $\rho_V = V/4\pi G_*$ and $P_V = -\rho_V$ and $\rho_T = \rho_* + \rho_V$, $P_T = P_* + P_V$. Using $\psi_* = H_*\varphi'_*$, we obtain

$$\frac{2}{3 - \varphi_*'^2}\varphi_*'' + \left(1 - \frac{P_T}{\rho_T}\right)\varphi_*' = -\alpha(\varphi_*)\frac{\rho_* - 3P_*}{\rho_T} - \alpha_V\frac{\rho_V - 3P_V}{\rho_T} \quad (73)$$

with $\alpha_V = d \ln V^{1/4}/d\varphi_*$.

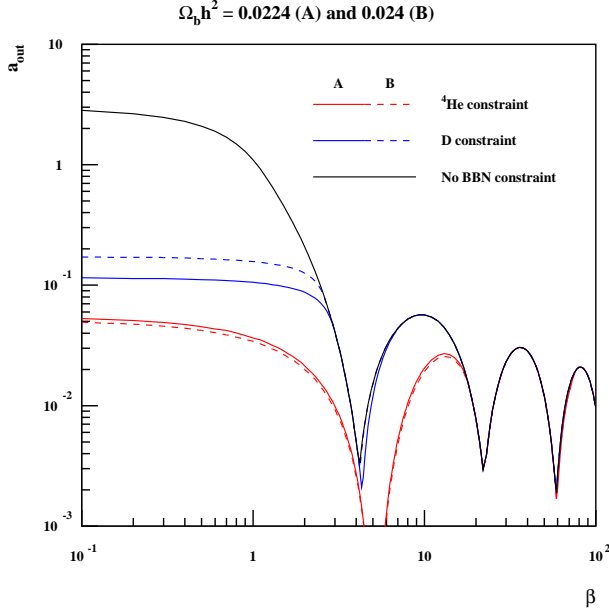


FIG. 19: Constraints in the plane (a_{out}, β) arising from D and ${}^4\text{He}$ BBN abundances. The upper line corresponds to the maximum value reached by a_{out} assuming $a_{\text{in}} = 0 - 2$. The middle line corresponds to the constraint obtained when D abundances are taken into account while the lower line corresponds to the constraint from ${}^4\text{He}$ abundances. We conclude that ${}^4\text{He}$ alone is sufficient to set the constraints on the model and that for $\beta \gtrsim 20$, all models with reasonable a_{in} are compatible with BBN.

B. Constant potential in the Einstein frame

In this model, the dilaton remains massless and $\alpha_V = 0$. It follows that the Klein-Gordon equation for φ_* takes the same form as Eq. (44). The dynamics of the universe is just modified at late time due to the contribution of the constant potential to the Friedmann equation (see Fig. 22). It follows that our previous results for the relation between a_{in} and a_{out} are not affected and that the attraction mechanism operates similarly. In particular the constraints on the parameters (a_{out}, β) obtained in Fig. 19 remain unchanged and the constraints on the parameters (α_0, β) will be modified only by late time dynamics.

The value of V_0 is fixed by

$$\Omega_{\Lambda 0} = \frac{2V_0}{3H_0^2 A_0^2} \quad (74)$$

and it dominates only during the last e -fold or so. The field is damped during the matter era so that it will be slow-rolling close to present time. It follows that $\varphi''_* \ll \varphi'$ so that

$$(1 + \Omega_V)\varphi'_{*0} \sim -\alpha_0 \Omega_{\text{mat}}. \quad (75)$$

Using WMAP concordance values, one finds $\varphi'_{*0} \sim$

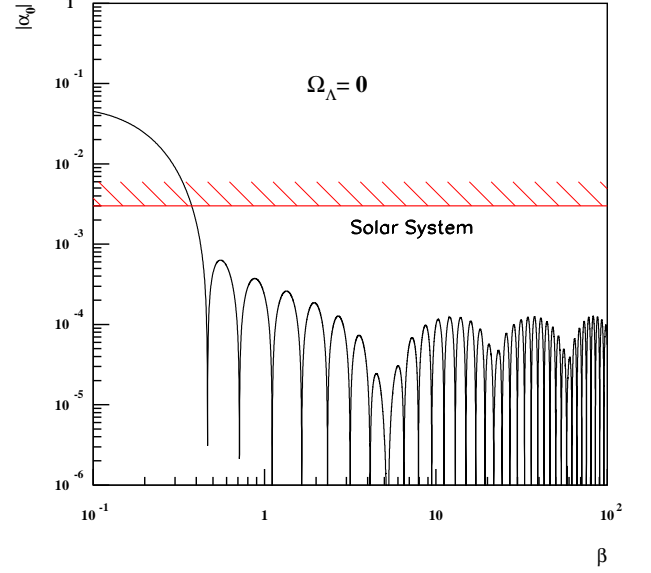


FIG. 20: Constraints on (α_0, β) from ${}^4\text{He}$ observations only (See Fig. 19) using WMAP measurement of Ω_b . The dashed line represents the constraint obtained in the Solar System.

$-0.2\alpha_0$ so that the constraint (32) on the time variation of G_{cav} is satisfied, simply because α_0 is small.

As a consequence, we expect the effect of an Einstein-frame cosmological constant is a shift in the global constraint contour obtained previously when $V = 0$. Figure 21 gives the new bounds set by BBN in the (α_0, β) plane.

C. Constant potential in Jordan frame

When one adopts a cosmological constant in the Jordan frame, the dilaton is not massless anymore and the value of U_0 is fixed by the constraint

$$\Omega_{\Lambda 0} = \frac{U_0 A_0^2}{3H_0^2}. \quad (76)$$

The coupling $\alpha_V = \alpha$. As in the previous case, the potential will dominate only during the last e -fold. In the slow-roll regime

$$(1 + \Omega_V)\varphi'_{*0} \sim -\alpha_0(\Omega_{\text{mat}} + \Omega_V). \quad (77)$$

With the concordance values, this implies that $\varphi'_{*0} \sim -0.6\alpha_0$ so that, again, the constraint (32) on the time variation of G_{cav} is satisfied. As shown in Fig. 22, these two models only differ at late times and figure 21 gives the new bounds set by BBN in the (α_0, β) plane.

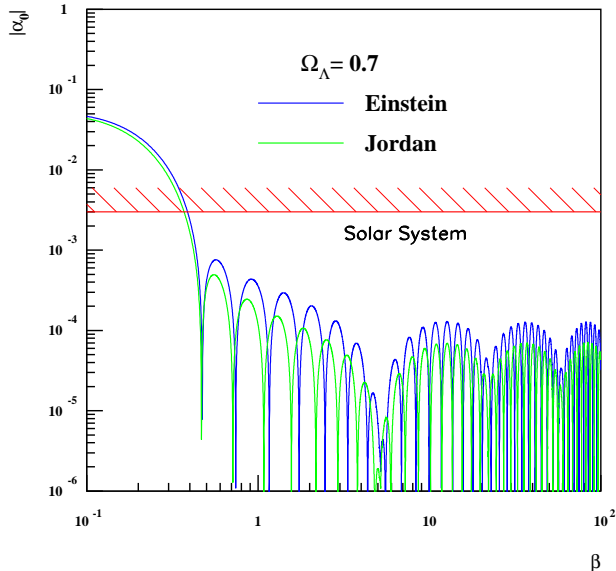


FIG. 21: Same as Fig. 20 but with a cosmological constant either in Einstein frame or Jordan frame.

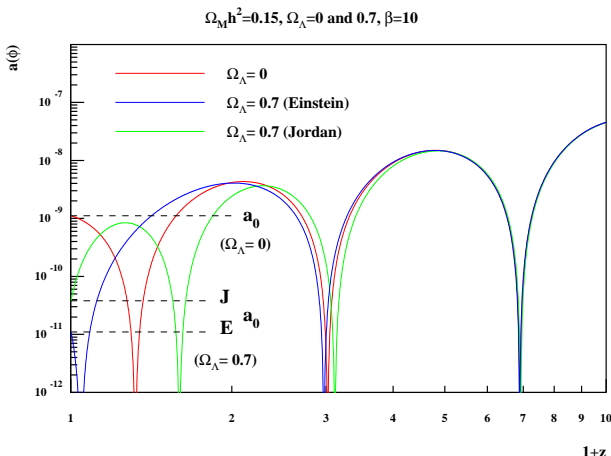


FIG. 22: Evolution of the scalar field as a function of z in models with a vanishing cosmological constant and a cosmological constant defined either in Einstein or Jordan frame. We see that only the late time dynamics is affected by the cosmological constant.

V. CONCLUSIONS

This article described the implementation of general scalar-tensor theories applicable to a BBN code. The

formalism allows one to choose any self-interaction potential as well as any coupling to matter. As such it can be applied to models which account for the present day acceleration such as (extended) quintessence models.

The ability to use BBN as a constraint completes our set of tools, which include CMB anisotropies and SNIa [16] and weak lensing [21], to study the cosmological imprints of this set of well-motivated theories of gravity. All observables are computed using the same formalism for compatibility. They can be used conjointly to set constraints on these theories and on deviations from general relativity during the entire evolution of our universe. We emphasize their complementarity since BBN depends only on the background evolution and mainly tests the attraction mechanism toward GR, CMB is mainly sensitive to the evolution of the perturbations in the linear regime while weak lensing probes the non-linear regime.

In this article, we have focused on the case of a quadratic coupling in order to check our code. In the case where $V = 0$ our results are compatible with previous analysis [35]. Note however that they do not rely on any specific form of the analytic solution. Also, our evaluation of the Fermi integrals that are necessary to estimate the kick during electron-positron annihilation do not rely on an approximation but rather on a full numerical integration. We have used a complete BBN code with up to date nuclear reaction rates. Current data on the light element abundances have been used to set constraints and we have also investigated the effect of a cosmological constant on these constraints. For this particular model, CMB anisotropies are not affected and we are allowed to infer Ω_b from standard CMB analyses. We emphasize that in general this has to be checked case by case.

Since our approach is fully numerical, it can be applied to any scenario and in particular to extended quintessence scenarios such as models with runaway fields. In these models, during the radiation era, the field evolves to reach a scaling solution. Before this, there may be a kinetic phase. According to when this kinetic phase ends, various effects on BBN can be expected. In particular $\varphi_{*in} = \text{const.}$ may not be a good approximation. It was also proposed that the coupling to dark matter may be different to the coupling to standard matter. This hypothesis relaxes the Solar system bound and allows higher values of α_{cdm} . All these questions, and others, will be addressed in following works.

Acknowledgements: We would like to thank T. Damour, G. Esposito-Farèse and C. Schimd for discussions and comments. The work of K.A.O. was supported in part by DOE grant DE-FG02-94ER-40823. The work is also supported by the project “INSU-CNRS/USA”.

[1] P.J.E. Peebles and B. Ratra, Rev. Mod. Phys. **59**, 559 (2003).

[2] J.-P. Uzan, N. Aghanim, and Y. Mellier, Phys. Rev. D **71**, (2005).

- [3] J.-P. Uzan, [arXiv:astro-ph/0409424].
- [4] R. Bean, S. Carroll, and M. Trodden, [arXiv:astro-ph/0510059].
- [5] P. Jordan, *Nature (London)* **164**, 637 (1956);
M. Fierz, *Helv. Phys. Acta* **29**, 128 (1956);
C. Brans and R. Dicke, *Phys. Rev. D* **124**, 925 (1961);
P.G. Bergmann, *Int. J. Theor. Phys.* **1**, 25 (1968);
K. Nordtvedt, *Astrophys. J.* **161**, 1059 (1970);
R. Wagoner, *Phys. Rev. D* **1**, 3209 (1970).
- [6] T. Damour and G. Esposito-Farèse, *Class. Quant. Grav.* **9**, 2093 (1992).
- [7] J. Polchinsky, *String theory* (Cambridge University Press, 1998).
- [8] T. Damour and K. Nordtvedt, *Phys. Rev. Lett.* **70** (1993) 2217; *Phys. Rev. D* **48**, 3436 (1993).
- [9] T. Damour and A.M. Polyakov, *Nuc. Phys. B* **423**, 532 (1994).
- [10] J.-P. Uzan, *Phys. Rev. D* **59**, 123510 (1999).
- [11] T. Chiba, *Phys. Rev. D* **60**, 083508 (1999);
L. Amendola, *Phys. Rev. D* **62**, 043511 (2000); A. Riazuelo and J.-P. Uzan, *Phys. Rev. D* **62**, 083506 (2000).
- [12] N. Bartolo and M. Pietroni, *Phys. Rev. D* **61**, 023518 (2000).
- [13] M. Gasperini, F. Piazza, and G. Veneziano, *Phys. Rev. D* **66**, 023528 (2002).
- [14] T. Damour, F. Piazza, and G. Veneziano, *Phys. Rev. D* **66**, 081601 (2002).
- [15] J. Martin, C. Schmid, and J.-P. Uzan, [arXiv:astro-ph/0510208].
- [16] A. Riazuelo and J.-P. Uzan, *Phys. Rev. D* **66**, 023525 (2002).
- [17] F. Perrotta, C. Baccigalupi, and S. Matarrese, *Phys. Rev. D* **61**, 023507 (2000).
- [18] L. Amendola, *Phys. Rev. Lett.* **86**, 196 (2001).
- [19] C. Baccigalupi, S. Matarrese, and F. Perrotta, *Phys. Rev. D* **62**, 123510 (2000).
- [20] X. Chen and M. Kamionkowski, *Phys. Rev. D* **60**, 104036 (1999).
- [21] C. Schmid, J.-P. Uzan, and A. Riazuelo, *Phys. Rev. D* **71**, 083512 (2005).
- [22] V. Acquaviva, C. Baccigalupi, and F. Perrotta, *Phys. Rev. D* **70**, 023515 (2004).
- [23] T. P. Walker *et al.*, *Ap.J.* **376**, 51 (1991);
K. A. Olive, G. Steigman, and T. P. Walker, *Phys. Rep.* **333**, 389 (2000);
B. D. Fields and S. Sarkar, *Phys. Rev. D* **66**, 010001 (2002).
- [24] R. H. Cyburt, B. D. Fields and K. A. Olive, *New Astron.* **6** 215 (1996); Coc, A. *et al.*, *Phys. Rev. D* **65**, 043510 (2002).
- [25] C. L. Bennett *et al.*, *Astrophys. J. Suppl.* **148**, 1 (2003);
D. N. Spergel *et al.*, *Astrophys. J. Suppl.* **148**, 175 (2003).
- [26] R. H. Cyburt, B. D. Fields and K. A. Olive, *Phys. Lett. B* **567**, 227 (2003).
- [27] A. Coc *et al.*, *Astrophys. J.* , **600**, 544 (2004).
- [28] P. Descouvemont *et al.*, *ADNDT* **88**, 203 (2004).
- [29] A. Cuoco *et al.*, *Int. J. Mod. Phys. A* **19** 4431 (2004).
- [30] R. H. Cyburt, *Phys. Rev. D* **70**, 023505 (2004).
- [31] R. H. Cyburt, B. D. Fields, K. A. Olive and E. Skillman, *Astropart. Phys.* **23**, 313 (2005).
- [32] J.-P. Uzan, *Rev. Mod. Phys.* **75**, 403 (2003).
- [33] J.D. Barrow, *Month. Not. R. Astron. Soc.* **184**, 677 (1978);
J. Yang *et al.*, *Astrophys. J.* **277**, 697 (1979);
F.S. Acceta *et al.*, *Phys. Lett. B* **248**, 94 (1990).
- [34] J.D. Barrow, *Month. Not. R. Astron. Soc.* **184**, 479 (1978);
J. Yang *et al.*, *Astrophys. J.* **227**, 697 (1979);
K. Arai, M. Hashimoto, and T. Fukui, *Astron. Astrophys.* **179**, 17 (1987);
F.S. Accetta, L.M. Krauss, and P. Romanelli, *Phys. Lett. B* **248**, 146 (1990);
T. Damour and C. Gundlach, *Phys. Rev. D* **43**, 3873 (1991);
J. A. Casas, J. Garcia-Bellido and M. Quiros, *Mod. Phys. Lett. A* **7**, 447 (1992);
J. A. Casas, J. Garcia-Bellido and M. Quiros, *Phys. Lett. B* **278**, 94 (1992);
T. Clifton, J.D. Barrow, and R.J. Scherrer, [arXiv:astro-ph/0504418].
- [35] T. Damour and B. Pichon, *Phys. Rev. D* **59**, 123502 (1999).
- [36] D.I. Santiago, D. Kalligas, and R.V. Wagoner, *Phys. Rev. D* **56**, 7627 (1997).
- [37] A. Serna and J.M. Alimi, *Phys. Rev. D* **53**, 3074 (1996);
Phys. Rev. D **53**, 3087 (1996).
- [38] C.J. Copi, A.N. Davis, and L.M. Krauss, *Phys. Rev. Lett.* **92**, 171301 (2004).
- [39] J.P. Kneller and G. Steigman, *Phys. Rev. D* **64**, 063501 (2003).
- [40] C. Will *Theory and experiments in gravitational physics* (Cambridge University Press, Cambridge, England, 1993); C. Will *Living Rev. Rel.* **4**, 4 (2001).
- [41] I.I. Shapiro, in *General Relativity and Gravitation 12*, N. Ashby *et al.* Eds. (Cambridge University Press, 1990), pp. 313.
- [42] J.G. Williams, X.X. Newhall, and J.O. Dickey, *Phys. Rev. D* **53**, 6730 (1996).
- [43] S.S. Shapiro *et al.*, *Phys. Rev. Lett.* **92**, 121101 (2004).
- [44] B. Bertotti, L. Iess, and P. Tortora, *Nature (London)* **425**, 374 (2003).
- [45] G. Esposito-Farèse and D. Polarski, *Phys. Rev. D* **63**, 063504 (2001).
- [46] T. Damour and G. Esposito-Farèse, *Phys. Rev. D* **54**, 1474 (1996).
- [47] J.O. Dickey *et al.*, *Science* **265**, 482 (1994).
- [48] J. Barker, *Astrophys. J.* **219**, 5 (1978).
- [49] N. Kaloper and K. A. Olive, *Astropart. Phys.* **1**, 185 (1993); A. A. Tseytlin, *Int. J. Mod. Phys. D* **1**, 223 (1992).
- [50] E. Kolb and M. Turner, *The early universe* (Addison Wesley, 1993);
P. Peter and J.-P. Uzan, *Cosmologie primordiale* (Belin, 2005).
- [51] J. Larena *et al.*, [arXiv:astro-ph/0511693].
- [52] S. Burles and D. Tytler, *Astrophys. J.* **499**, 699 (1998);
ibid. **507**, 732 (1998).
- [53] J. M. O'Meara *et al.* *Astrophys. J.* **552**, 718 (2001).
- [54] D. Kirkman *et al.*, *Astrophys. J. Suppl.* **149**, 1 (2003).
- [55] M. Pettini and D. V. Bowen, *Astrophys. J.* **560**, 41 (2001).
- [56] Y. I. Izotov, T. X. Thuan, and V. A. Lipovetsky, *Astrophys. J.* **435**, 647 (1994) 647;
ibid., **108**, 1. (1997) 1;
Y. I. Izotov and T. X. Thuan, *Astrophys. J.* **500**, 188 (1998).
- [57] Y. I. Izotov and T. X. Thuan, *Astrophys. J.* **602**, 200 (2004).

- [58] K.A. Olive, and E. Skillman, *New Astron.* **6**, 119 (2001).
- [59] K. A. Olive and E. D. Skillman, *Astrophys. J.* **617**, 29 (2004).
- [60] S.G. Ryan *et al.*, *Astrophys. J. Lett.* **530**, L57 (2000).
- [61] J. Melendez and I. Ramirez, *Astrophys. J.* **615**, L33 (2004) L33.